Applied Catalysis B: Environmental 180 (2016) 656–662

Contents lists available at ScienceDirect

Applied Catalysis B: Environmental

journal homepage: www.elsevier.com/locate/apcatb

Carbon dots decorated graphitic carbon nitride as an efficient metal-free photocatalyst for phenol degradation

Hui Zhang, Lixia Zhao, Fanglan Geng, Liang-Hong Guo*, Bin Wan, Yu Yang

State Key Laboratory of Environmental Chemistry and Eco-toxicology, Research Centre for Eco- environmental Sciences, Chinese Academy of Sciences, 18 Shuangqing Road, P.O. Box 2871, Beijing 100085, China

ARTICLE INFO

Article history:
Received 13 April 2015
Received in revised form 23 June 2015
Accepted 25 June 2015
Available online 17 July 2015

Keywords:
Carbon dot
Graphitic carbon nitride
Metal-free photocatalyst
Phenol

ABSTRACT

Environment-friendly metal-free photocatalysts represent a promising alternative to conventional metal-based semiconductors. In this report, a carbon dots (CDs) decorated graphitic carbon nitride (g-C_3N_4) photocatalyst was synthesized via a facile impregnation-thermal method. Under visible light irradiation, a very low CDs content of 0.5 wt% in the g-C_3N_4/CDs composite resulted in a 3.7 times faster reaction rate for phenol photodegradation than pristine g-C_3N_4. Spectroscopic and photoelectrochemical characterizations revealed that impregnation of CDs into g-C_3N_4 not only enhanced the production of photogenerated electron-hole pairs by extending the visible light absorption region due to the upconverted photoluminescence character of CDs, but also facilitated electron-hole separation by band alignment in the g-C_3N_4/CDs junction, thus yielded more holes, $^{\bullet}O_2^-$ and $^{\bullet}OH$ radicals to promote phenol degradation. These results highlight the potential application of sustainable metal-free photocatalysts in water purification.

© 2015 Elsevier B.V. All rights reserved.

1. Introduction

Sunlight-driven photocatalytic reactions represent a promising way to address the increasing environmental and energy concerns [1–4]. From the viewpoint of solar-energy use, photocatalytic performance strongly depends on the semiconductor's absorption capacity toward sunlight and the reaction efficiency of photogenerated charge carriers. To date, various visible-light-sensitive semiconductors, including multi-metal oxides, sulfides and oxynitrides, have been successfully fabricated by band-structure engineering [5–8]. Nevertheless, considering the side issues such as scalability and sustainability, earth-abundant metal-free semiconductors are greatly desired. As a sustainable material, graphitic carbon nitride (g-C_3N_4) represents an attractive visible light photocatalyst because of its suitable band gap (2.7 eV) for sunlight absorption and outstanding catalytic activity [9]. The high chemical stability of g-C_3N_4 together with the low cost of mass production makes it an ideal candidate for applications like photocatalytic water splitting, CO_2 reduction and pollutant degradation [10–14]. However, despite great progress in g-C_3N_4 synthesis, the weak van der Waals interactions between adjacent CN layers in g-C_3N_4 impede charge transfer and separation, and thus impose severe limitations on the photocatalytic performance.

One promising strategy to enhance the photocatalytic performance of g-C_3N_4 is to form surface junctions to promote charge separation. Two typical approaches have been developed to construct effective surface junctions. One is to decorate g-C_3N_4 with metal nanoparticles (e.g., Au and Ag) or carbon nanomaterials (e.g., carbon nanotube and graphene), which can effectively capture photogenerated electrons in g-C_3N_4 and improve catalytic efficiency [15–18]. The other promising approach is to construct semiconductor heterojunctions with a suitable band- alignment structure, such as CdS and Cu_2O [19–23] . Such structures can simultaneously optimize light capture and facilitate charge separation at the interface between the two semiconductors. It is noted that the formation of effective junctions strongly depends on the crystal structure, band structure, electron affinity and interfacial contact of both materials. However, the main problem of these composites is the leaching of toxic metals during photocatalytic processes. Photocatalytic systems based on metal-free, sustainable materials are highly desirable for large-scale photocatalytic applications.

Recently, carbon dots (CDs), which are predominantly composed of graphitic carbon (sp^2 carbon) with a size below 10 nm, have attracted considerable attention because of their unique optical and electronic properties [24,25]. The quantum effect endows CDs with broad-band optical absorption. Thus, CDs have been

* Corresponding author.
E-mail address: LHGuo@rcees.ac.cn (L.-H. Guo).

http://dx.doi.org/10.1016/j.apcatb.2015.06.056
0926-3373/© 2015 Elsevier B.V. All rights reserved.

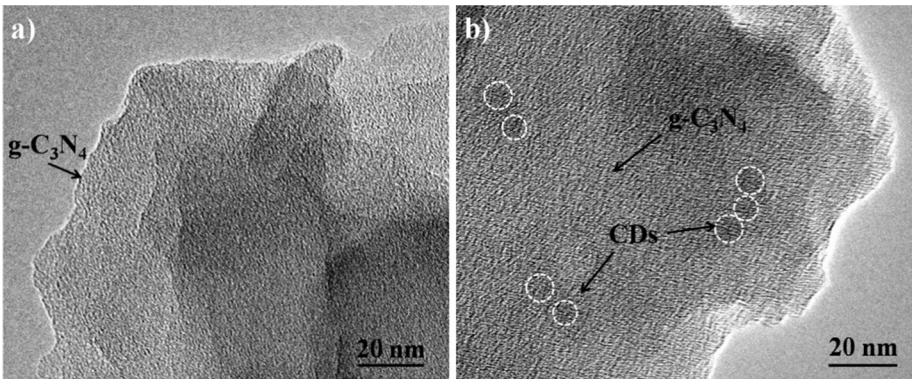

Fig. 1. TEM images of (a) g-C_3N_4 and (b) g-C_3N_4/CDs (0.5 wt%) composite.

widely used as light absorbers to couple with semiconductor nanoparticles, such as TiO_2, Si and Ag_3PO_4, to improve their photocatalytic performance [26–28]. In addition, CDs also act as an electron acceptor or transporter to direct the flow of photogenerated charge carriers [29] . Considering the analogous π–conjugated structure of g-C_3N_4 and CDs, the combination of these two materials is expected to deliver high photocatalytic performance.

With the above merits, we report an earth-abundant, metal-free g-C_3N_4/CDs heterojunction synthesized by directly coating CDs onto the g-C_3N_4 surface. The CDs decorated g-C_3N_4 composite exhibited greatly enhanced photocatalytic activity toward phenol degradation under visible light irradiation compared with that of g-C_3N_4. The role of the CDs in the composite was systemically investigated. The metal-free and environment-friendly properties of the g-C_3N_4/CDs composite make it a promising photocatalytic system for practical applications.

2. Experimental

2.1. Chemicals and materials

Cyanamide was purchased from Alfa Aesar (Ward Hill, MA, USA). Phenol was purchased from Sigma- Aldrich (St. Louis, MO, USA). 5,5-Dimethyl-1-pyrroline-N-oxide (DMPO) was obtained from Dojindo Laboratories (Kumamoto, Japan). Methanol was obtained from Fisher Scientific (Pittsburgh, PA, USA). All other chemicals were of analytical grade and used without further purification. All solutions were freshly prepared with deionized water (resistivity: 18.2 MΩ) obtained using a Millipore Milli-Q water purification system (Bedford, MA, USA).

2.2. Synthesis of g-C_3N_4

Pure g-C_3N_4 was prepared by a simple calcination method according to the literature [30]. Cyanamide was put into a quartz boat and heated in static air to 520 °C (ramp rate: 2 °C/min) and then kept for 4 h. The yellow g-C_3N_4 product was collected and ground into powder with an agate mortar for further use.

2.2.1. Synthesis of g-C_3N_4/CDs nanocomposite

CDs were synthesized by the pyrolysis of citric acid and branched poly(ethylenimine) according to our previous report [31]. A typical preparation of g-C_3N_4/CDs nanocomposite was as follows: g-C_3N_4 (0.2 g) and a certain volume of CDs aqueous solution (1 mg mL^{-1}) were mixed and vigorously stirred for 24 h, followed by vaporizing the solvent at 100 °C in an electric thermostatic drying oven. The as-obtained powder was calcined at 300 °C for 1 h at ambient conditions. Following the same procedure, different mass ratios of g-C_3N_4/CDs nanocomposites with 0.1 wt%, 0.2 wt%, 0.5 wt% and 1 wt% CDs, respectively, were synthesized.

2.3. Characterization

The morphology of the synthesized photocatalysts was examined by transmission electron microscopy (TEM) using a JEOL 2100F instrument (Tokyo, Japan) operated at an accelerating voltage of 200 kV. X-ray photoelectron spectroscopy (XPS) data were obtained on a Thermo VG ESCALAB 250 spectrometer (East Grinsted, UK) with Al Kα radiation at 1486.6 eV. Fourier transform infrared (FTIR) spectra were recorded on a JASCO 6100 spectrophotometer (Japan). UV–vis diffuse reflectance measurements were performed on a Varian Cary 5000 spectrometer (Palo Alto, CA, USA). Fluorescence spectra were obtained on a Horiba Fluoromax-4spectrofluorimeter (Edison, NJ, USA). The total organic carbon (TOC) was measured using a multi N/C 3000 analyzer (Analytik Jena AG, Germany). Electron spin resonance (ESR) signal of radicals spin-trapped by DMPO was recorded on a Bruker ER073 spectrometer (Karlsruhe, Germany) during visible light irradiation of the suspension (0.05 mg mL^{-1} photocatalyst, 100 mM DMPO). The settings for ESR measurements were as follows: center field 3503.95 G, microwave frequency 9.84 GHz, and power 20 mW. Photoelectrochemical measurements were performed in a three-electrode quartz cell on a CHI 630B electrochemical workstation (Shanghai, China). A Pt plate and Ag/AgCl electrode were used as the counter electrode and reference electrode, respectively. The working electrodes were prepared by spreading a slurry of the as-prepared photocatalyst onto the fluorine-doped tin oxide (FTO) glass. Photocurrent-time curves were measured in 0.1 M Na_2SO_4 electrolyte. Electrochemical impedance spectra (EIS) were measured in 0.1 M KCl solution containing 2.5 mM $K_3[Fe(CN)_6]/K_4[Fe(CN)_6]$ (1:1) with a sinusoidal ac perturbation of 5 mV over a frequency range of 1 MHz to 100 mHz.

2.4. Photocatalytic performance evaluation

Photodegradation of a phenol solution (10 mg L^{-1}) was performed to evaluate the photocatalytic performance of the synthesized catalysts, which was carried out in a top-window Pyrex cell with the temperature maintained at 20 °C by a circulating water system. The catalyst (50 mg) was added into the phenol solution (50 mL). Prior to irradiation, the suspension was magnetically stirred in the dark for 30 min to ensure phenol adsorption/desorption equilibrium. Then, the suspension was irradiated by a 300 W Xe lamp with a cut off filter (<400 nm) and an irradiation intensity of 100 mW cm^{-2}. At given time intervals, aliquots of the irradiated suspension were collected, centrifuged and analyzed on an Aligent 1260 high-performance liquid chromatography (HPLC) (Palo Alto, CA, USA) with a Poroshell 120 EC-C18 column.

The detection wavelength was at 280 nm. The mobile phase was a mixture of methanol and water with a volume ratio of 55:45 and flow rate of 0.3 mL min^{-1}.

3. Results and discussion

3.1. Structural characterization of g-C_3N_4/CDs composites

TEM images showed that the as-prepared CDs were monodispersed with an average diameter of 3.6 nm (Fig. S1). The light-brown CDs solution displayed a broad optical absorption below 500 nm with a peak at 355 nm. The photoluminescence emission of CDs exhibited an excitation wavelength dependent behavior due to the existence of different emissive states of CDs (Fig. S2) [32]. The excellent dispersibility of the CDs in water originated from the numerous oxygen- functional groups on their surface. As observed from Fig. 1, the pristine g-C_3N_4 displayed a typical layered structure. For the g-C_3N_4/CDs composite sample, CDs adhered to the g-C_3N_4 surface, which may arise from π–π stacking interactions [16,17].

The interaction between the CDs and g-C_3N_4 was first investigated by FTIR spectra. As shown in Fig. S3, the band at 810 cm^{-1} could be attributed to the breathing mode of triazine units [33]. The bands in the 1200–1600 cm^{-1} region were corresponding to the stretching vibration of the CN heterocycle [34]. Notably, these bands in the g-C_3N_4/CDs composite depicted slight red-shifts as compared to those in the pristine g-C_3N_4, e.g., 1249 → 1237 cm^{-1}, 1328 → 1321 cm^{-1}, 1415 → 1406 cm^{-1} and 1570 → 1568 cm^{-1}, suggesting the bond strength of C—N was weakened due to the strong interaction between the CDs and g-C_3N_4 in the composites [33,34]. XPS spectra were further performed to comprehend the interactions (Fig. 2). The N 1s spectra of both g-C_3N_4 and g-C_3N_4/CDs composite presented the typical tertiary N—$(C)_3$ groups (399.8 eV) and triazine rings (398.5 eV) [35]. Interestingly, a new shoulder peak at 397.6 eV was obviously observed in g-C_3N_4/CDs composite, which might be caused by the significant interaction between the CDs and the N atoms in the g-C_3N_4 [23]. The C 1s spectra of the g-C_3N_4 could be deconvoluted into two species: sp^2–bonded C atoms N—C═N (288.1 eV) and C═C (284.6 eV). The two new peaks in g-C_3N_4/CDs composite was attributed to C—OH (285.7) and COOH (289.1 eV) species in CDs [31]. These results suggest the π–π stacking interaction between g-C_3N_4 and CDs should be responsible for the assembly of g-C_3N_4/CDs composites. Such noncovalent interactions between the two components prevent the formation of defects at the junction interface and thus give rise to a high-quality contact interface.

The optical absorption properties of the resultant g-C_3N_4/CDs composites were examined with UV–vis diffuse reflectance spectroscopy (Fig. 3a). Pristine g-C_3N_4 exhibited an intrinsic absorption edge at 460 nm with a calculated band gap of 2.7 eV according to the Kubelka-Munk function [36]. After the introduction of CDs, the absorption edge of g-C_3N_4 did not shift, which suggested that the CDs were probably anchored onto the surface of g-C_3N_4 and therefore did not change its bulk optical properties. The visible light harvesting capability of the g-C_3N_4/CDs composites increased with the CDs content due to the intrinsic optical absorbance of the CDs. Indeed, CDs can absorb visible light with longer wavelength (>550 nm) and then emit photoluminescence at a shorter wavelength (400–500 nm) due to the upconverted photoluminescence property (Fig. 3b), which can be attributed to a multiphoton active process [26,37]. These results suggest that CDs can serve as a light harvesting component for g-$C_3N_4$to improve visible light utilization, which should enhance the photocatalytic performance of the g-C_3N_4/CDs composites under sunlight.

3.2. Photocatalytic performance of g-C_3N_4/CDs composites

The photocatalytic performance of the synthesized catalysts was evaluated by phenol degradation experiments, which is a typical intermediate in the degradation of aromatic hydrocarbons and is difficult to degrade using conventional degradation technologies. As shown in Fig. 4a, phenol was stable under visible light irradiation in the absence of a photocatalyst. After the addition of g-C_3N_4 or g-C_3N_4/CDs composites, phenol degradation occurred upon light irradiation. Greatly enhanced phenol degradation was observed upon the introduction of CDs onto g-C_3N_4. For the composite containing 0.5 wt% CDs, the phenol solution was completely degraded within 200 min, whereas only about 50% phenol was decomposed over the pristine g-C_3N_4 sample during the same period. To quantitatively analyze the catalytic efficiency, the phenol degradation rates were extracted by assuming pseudo-first-order kinetics (Fig. 4b). All the g-C_3N_4/CDs catalysts exhibited 1.9 to 3.7 times higher rate constants than the pristine g-C_3N_4, indicating that CDs indeed boosted the photocatalytic activity of g-C_3N_4.

The wavelength-dependent phenol degradation experiments were further conducted to investigate the effect of the increased absorption induced by CDs (as shown in Fig. 3a) on the photocatalytic efficiency. Fig. S4 showed the phenol degradation efficiency over the g-C_3N_4/CDs catalysts under different light wavelength. For light with 450 ± 20 nm wavelength, an increasing photocatalytic activity toward phenol degradation was observed with increased CDs content (<0.5 wt%), which was similar to that under the whole visible light region. For light with 550 ± 20 nm wavelength, although g-C_3N_4 only absorb <460 nm light, phenol degradation still occurred in the presence of g-C_3N_4/CDs catalysts, which should be attributed to the CDs upconversion [22]. These results suggest that CDs would increase light harvesting capability of the g-C_3N_4/CDs composites and then promote the phenol degradation. However, the photocatalytic activity of g-C_3N_4/CDs composites dramatically decreased with CDs contents exceeded 0.5 wt%. This decrease is likely related to the "shielding effect" of the carbon material, which reduces light absorption and masks the active sites of the catalyst [17,38]. The highest photocatalytic activity was obtained for the composite with 0.5 wt% CDs, which was therefore used in subsequent experiments and labeled as g-C_3N_4/CDs.

The main intermediate products during the phenol photodegradation were displayed in Fig. 5a. Three typical intermediates including catechol, hydroquinone and *p*-benzoquinone were clearly observed. The concentration of these intermediates reached a maximum and then gradually declined with the irradiation time due to the ring cleavage process. The formed organic acids were further degraded to CO_2 and H_2O. This is consistent with the previous studies on phenol degradation by the •OH attack [39,40]. The proposed phenol photodegradation pathways were illustrated in Fig. S5. To further demonstrate the mineralization degree of phenol during photodegradation process, the evolution of TOC during light irradiation was investigated (Fig. 5b). Similarly, about 87% of phenol was mineralized to CO_2 within 200 min in the presence of g-C_3N_4/CDs composites. For comparison, the TOC value was only reduced by 43% for the pristine g-C_3N_4 during the same period. This indicates the g-C_3N_4/CDs composites possessed much higher mineralization efficiency for phenol photodegradation than g-C_3N_4 catalyst.

Considering the importance of photocatalyst stability in practical applications, the reusability of the g-C_3N_4/CDs composites for phenol degradation was evaluated (Fig. 6). Over five consecutive cycles, no obvious deactivation of the photocatalyst was observed. TEM analysis indicated that the distribution and density of CDs on the g-C_3N_4 surface were indistinguishable from those of the unused sample after photocatalytic cycle (Fig. S6). These results clearly

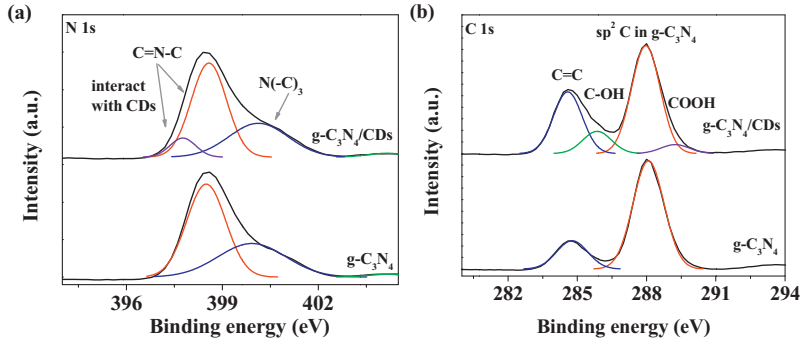

Fig. 2. (a) N 1s and (b) C 1s XPS spectra of g-C_3N_4 and g-C_3N_4/CDs (0.5 wt%) composite.

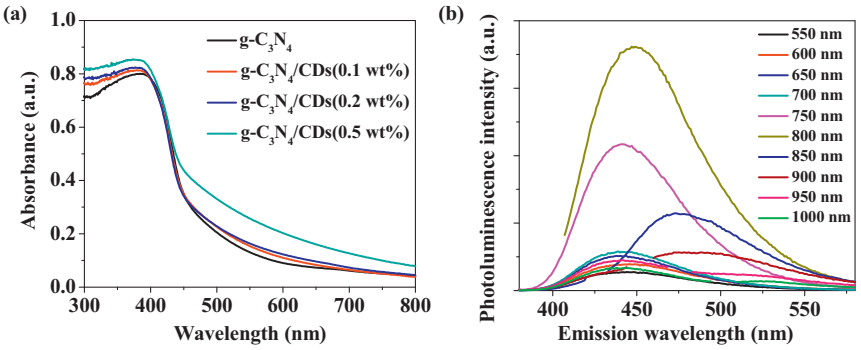

Fig. 3. (a) UV–vis diffuse reflectance absorbance spectra of g-C_3N_4 and g-C_3N_4/CDs composites. (b) Upconverted photoluminescence spectra of CDs with different excitation wavelength.

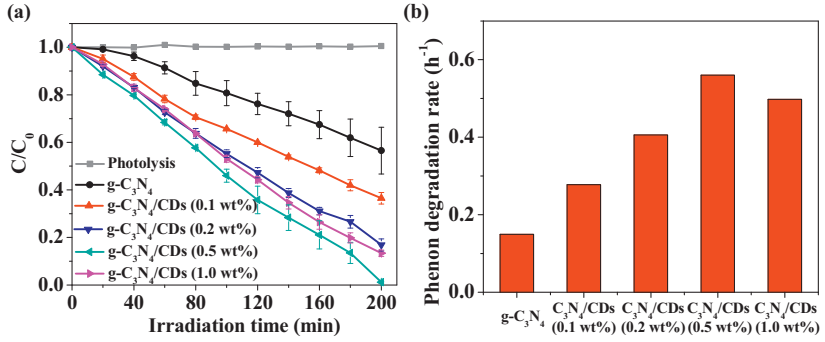

Fig. 4. (a) Temporal evolution of phenol concentration in g-C_3N_4 and g-C_3N_4/CDs suspensions under visible light irradiation (λ > 400 nm). (b) Apparent rate constants of phenol degradation over different photocatalysts.

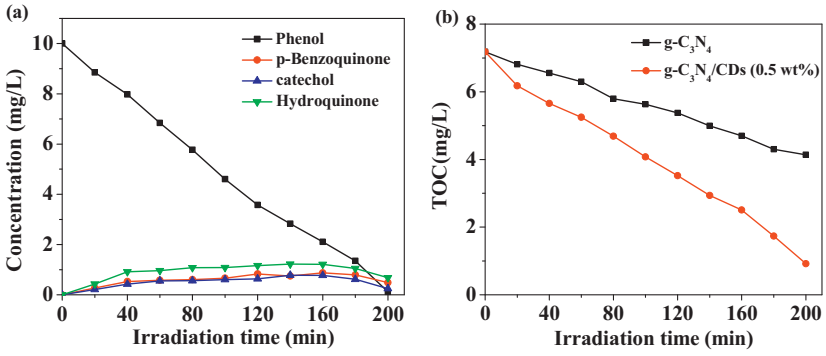

Fig. 5. (a) Temporal evolution of phenol and the hydroxylated phenolic intermediates in g-C_3N_4/CDs suspensions. (b) Temporal evolution of TOC concentration in g-C_3N_4 and g-C_3N_4/CDs suspensions under visible light irradiation (λ > 400 nm).

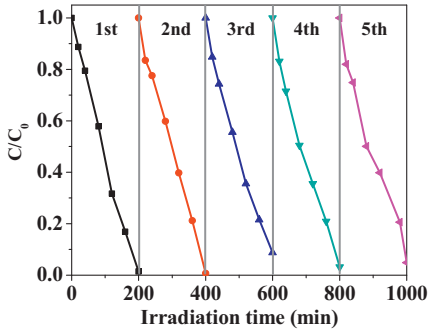

Fig. 6. Recycling performance ofg-C_3N_4/CDs composite towards phenol degradation under visible light irradiation (λ > 400 nm).

indicate the high- stability of the g-C_3N_4/CDs composite during the photocatalytic reaction.

3.3. Photocatalytic mechanism for g-C_3N_4/CDs composites

To elucidate the phenol degradation mechanism by the g-C_3N_4/CDs composite, the generation of reactive oxygen species (ROS) over the g-C_3N_4/CDs composite under visible light irradiation was probed by a DMPO spin-trapping ESR technique. As shown in Fig. 7, no ESR signal was observed in the dark. Upon visible light irradiation, a four-line ESR signal with an intensity ratio of 1:1:1:1was clearly observed, which is characteristic of DMPO— $^{\bullet}O_2^-$ adduct. The $^{\bullet}$OH radical was also captured to form DMPO— $^{\bullet}$OH adduct with a characteristic 1:2:2:1 quadruplet and spacing of 15G in the magnetic field [41]. Since the photogenerated holes in the valance band of g-C_3N_4 (E_{VB} = +1.40 V, vs. NHE) are incapable of oxidizing hydroxyl groups into $^{\bullet}$OH radicals (E ($^{\bullet}$OH/OH$^-$) = +1.99 V, vs. NHE) due to the more negative valance band potential [42], it is believed that the observed $^{\bullet}$OH radicals were generated from the $^{\bullet}O_2^-$ radicals by photochemical reaction. Time-dependent ESR signals were also measured under the same conditions, where the intensity of the ESR signal could imply the concentration of ROS generated in each catalyst suspension. The intensity of radical signals gradually enhanced in both catalysts as the irradiation time increased, indicating the important role of $^{\bullet}O_2^-$ and $^{\bullet}$OH radicals in degrading phenol. A notable observation came from the higher formation rates of $^{\bullet}O_2^-$ and $^{\bullet}$OH radicals in g-C_3N_4/CDs systems than in the g-C_3N_4 one. This trend is consistent with the observed phenol degradation rate, and demonstrates that more ROS could attack phenol molecules in the g-C_3N_4/CDs system and subsequently promote their degradation than in the g-C_3N_4 system.

In addition to the above ROS generation analysis, the transient photocurrent responses of g-C_3N_4 and g-C_3N_4/CDs composite were measured to examine the charge generation and recombination behaviors in these photocatalyst systems. The reproducible photocurrent responses during the "on-off" irradiation cycles in Fig. 8a confirmed the good stability of the g-C_3N_4 and g-C_3N_4/CDs photoelectrodes. Notably, the introduction of CDs resulted in about two-fold enhancement in the photocurrent density compared to that of the pristine g-C_3N_4 electrode. Because the photocurrent arises from the transport of photogenerated electrons to the back contact and the simultaneous capture of photogenerated holes by hole scavengers in the electrolyte, the enhanced photocurrent

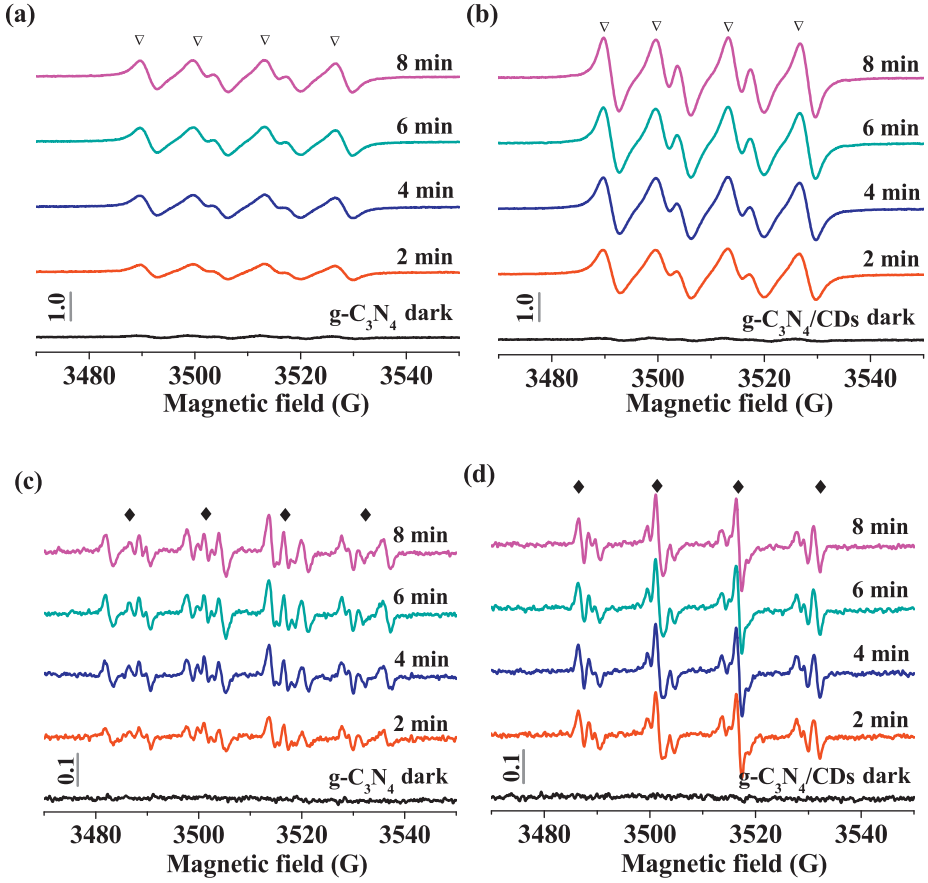

Fig. 7. ESR spectra of (a,b) DMPO— $^{\bullet}O_2^-$ adducts in methanol solution and (c, d) DMPO— $^{\bullet}$OH adducts in aqueous solution recorded with (a, c) g-C_3N_4 and (b, d) g-C_3N_4/CDs composite during visible light irradiation (λ > 400 nm). The characteristic signals of DMPO—$^{\bullet}O_2^-$ adducts and DMPO— $^{\bullet}$OH adducts were marked with ▽ and ♦ symbols, respectively.

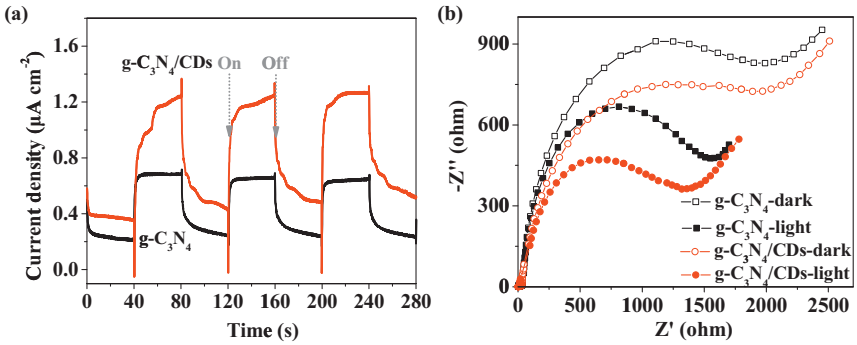

Fig. 8. (a) Transient photocurrent responses of g-C_3N_4 and g-C_3N_4/CDs photoelectrodes in 0.1 M Na_2SO_4 solution under 0 V bias potential (vs. Ag/AgCl). (b) Nyquist plots of g-C_3N_4 and g-C_3N_4/CDs photoelectrodes in 0.1 M Na_2SO_4 solution in the dark and under visible light irradiation (λ > 400 nm).

response of the g-C_3N_4/CDs electrode compared with the g-C_3N_4 electrode demonstrates that CDs promoted the efficient generation and separation of photogenerated electron-hole pairs, which are favorable for ROS generation and thus photocatalytic activity.

Another interesting observation came from the relatively slow photocurrent response of the g-C_3N_4/CDs sample during the "on-off" irradiation cycles. The delayed response of the composite electrode suggested that the CDs could capture and store the photoexcited electrons. A similar phenomenon has been observed in the carbon and noble-metal based composites [43,44]. Upon light irradiation, CDs could serve as electron reservoirs to store the photogenerated electrons, so only a portion of the photoelectrons are transported to the back contact electrode until the equilibrium state is reached. Thus, a gradually rising photocurrent response occurs. Similarly, the slow release of photoelectrons from the CDs could cause the slow response of the photocurrent delay curve when the irradiation is switched off. These results suggest that the photocarrier recombination is slower in the g-C_3N_4/CDs composite than in g-C_3N_4, which partly explains the markedly enhanced photocatalytic activity of the composites.

To validate the improved charge transfer behaviors of the g-C_3N_4/CDs, the EIS Nynquist plots of the two photoelectrodes in the dark and under illumination conditions were presented in Fig. 8b. The semicircle part at the high frequency region is associated with the charge-transfer process at the photoelectrode interface and a smaller radius implies more efficient charge transfer process [45]. Compared with the plot obtained in the dark, a much smaller radius was obtained under irradiation for both electrodes, consistent with the increased electron conductivity of the electrode under light. The semicircle in the Nyquist plot of the g-C_3N_4/CDs electrode exhibited a smaller radius than that of the g-C_3N_4 electrode, implying that interfacial charge transfer occurred more rapidly at the heterojunction interface of g-C_3N_4/CDs than in g-C_3N_4 and thus promoted efficient separation of the photogenerated electron-hole pairs.

Based on the above photocatalytic and photoelectrochemical analysis, a tentative mechanism for the enhanced photocatalytic performance of the g-C_3N_4/CDs composite was proposed, which is illustrated in Fig. 9. Under visible light irradiation, g-C_3N_4 could absorb light with wavelength <470 nm. Simultaneously, light of wavelength >550 nm could be converted to <470 nm light by the incorporated CDs, which subsequently excites g-C_3N_4 to generate electron-hole pairs [26] Importantly, the relative band alignment of g-C_3N_4 and CDs provides the feasibility of the migration of photoexcited electrons from g-C_3N_4 to CDs. These processes greatly inhibit the recombination of photogenerated charge carriers. Thus, the g-C_3N_4/CDs composite could not only promote charge generation by extending the absorption region toward sunlight spectra, but also facilitate charge separation and transport at the junction interface, which subsequently enhances the charge carrier generation and facilitate their reaction with the adsorbed species (such as O_2 and OH^-) to yield ROS (e.g.,$^{\bullet}O_2^-$, $^{\bullet}OH$), accelerating the phenol degradation.

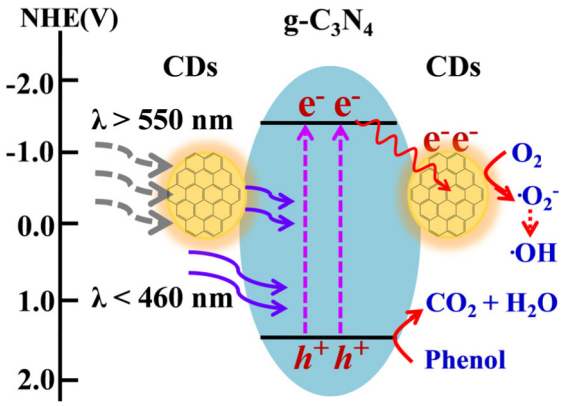

Fig. 9. Schematic illustration of the possible photocatalytic processes in the g-C_3N_4/CDs composite under visible light.

4. Conclusion

In summary, we developed a facile method to fabricate a metal-free g-C_3N_4/CDs photocatalyst to degrade organic contaminants. The similar π–π conjugated structure of the g-C_3N_4 and CDs components ensured the formation of a high-quality contact interface in the g-C_3N_4/CDs composite. Because of the extended visible light absorption range provided by the upconverted photoluminescence character of CDs and efficient charge separation arising from the energy alignment structure, the g-C_3N_4/CDs composite exhibited up to 3.7-fold enhancement in phenol degradation rate constant than that of the pristine g-C_3N_4 under visible light irradiation. This work will encourage new developments in metal-free photocatalysts and promote their practical application in environmental remediation.

Acknowledgments

This work was supported by the National Basic Research Program of China (2011CB936001) and National Natural Science Foundation of China (21321004, 21207146, 21177138, 21477146 and 21377142).

Appendix A. Supplementary data

Supplementary data associated with this article can be found, in the online version, at http://dx.doi.org/10.1016/j.apcatb.2015.06.056

References

[1] Z. Zou, J. Ye, K. Sayama, H. Arakawa, Nature 414 (2001) 625–627.
[2] A. Kudo, Y. Miseki, Chem. Soc. Rev. 38 (2009) 253–278.
[3] M.R. Hoffmann, S.T. Martin, W. Choi, D.W. Bahnemann, Chem. Rev. 95 (1995) 69–96.
[4] W.Y. Teoh, J.A. Scott, R. Amal, J. Phys. Chem. Lett. 3 (2012) 629–639.
[5] W.J. Jo, J.W. Jang, K.J. Kong, H.J. Kang, J.Y. Kim, H. Jun, K.P.S. Parmar, J.S. Lee, Angew. Chem. Int. Ed. 51 (2012) 3147–3151.
[6] F.X. Zhang, A. Yamakata, K. Maeda, Y. Moriya, T. Takata, J. Kubota, K. Teshima, S. Oishi, K. Domen, J. Am. Chem. Soc. 134 (2012) 8348–8351.
[7] X. Zong, G. Wu, H. Yan, G. Ma, J. Shi, F. Wen, L. Wang, C. Li, J. Phys. Chem. C 114 (2010) 1963–1968.
[8] H. Tong, S.X. Ouyang, Y.P. Bi, M. Oshikiri, N. Umezawa, M. Oshikiri, J.H. Ye, Adv. Mater. 24 (2012) 229–251.
[9] X.C. Wang, K. Maeda, A. Thomas, K. Takanabe, G. Xin, J.M. Carlsson, K. Domen, M.A. Antonietti, Nat. Mater. 8 (2009) 76–80.
[10] S. Chao, J. Yu, J. Phys. Chem. Lett. 5 (2014) 2101–2107.
[11] Y.J. Cui, Z.X. Ding, X.Z. Fu, X.C. Wang, Angew. Chem. Int. Ed. 51 (2012) 11814–11818.
[12] Y. Wang, Y. Shi, J. Lin, Y. Zhu, Energy Environ. Sci. 4 (2011) 2922–2929.
[13] Z. Lin, X. Wang, ChenSunChem 7 (2014) 1547–1550.
[14] Y. Zhen, L. Lin, X. Ye, F. Guo, X. Wang, Angew. Chem. Int. Ed. 53 (2014) 11926–11930.
[15] S. Samanta, S. Martha, K. Parida, ChemCatChem 6 (2014) 1453–1462.
[16] S.K. Bhunia, N.R. Jana, ACS Appl. Mater. Interfaces 6 (2014) 20085–20092.
[17] Y. Li, H. Zhang, P. Liu, D. Wang, Y. Li, H. Zhao, Small 9 (2013) 3336–3344.
[18] R.C. Pawar, S. Kang, S.H. Ahn, C.S. Lee, RSC Adv. 5 (2015) 24281–24292.
[19] J. Chen, S. Shen, P. Guo, M. Wang, B. Wu, X. Wang, L. Guo, Appl. Catal. B 152-153 (2014) 335–341.
[20] K. Chang, Z. Mei, T. Wang, Q. Kang, S. Ouyang, J. Ye, ACS Nano 8 (2014) 7078–7087.
[21] X. Wang, S. Blechert, M. Antonietti, ACS Catal. 2 (2012) 1596–1606.
[22] J. Zhang, M. Zhang, R.-Q. Sun, X. Wang, Angew. Chem. Int. Ed. 51 (2012) 10145–110149.
[23] J. Zhang, M. Zhang, L. Lin, X. Wang, Angew. Chem. Int. Ed. 54 (2015) 6297–6301.
[24] Y.P. Sun, B. Zhou, Y. Lin, W. Wang, K.A.S. Fernando, P. Pathak, M.J. Meziani, B.A. Harruff, X. Wang, H. Wang, P.G. Luo, H. Yang, M.E. Kose, B. Chen, L.M. Veca, S.Y. Xie, J. Am. Chem. Soc. 128 (2006) 7756–7757.
[25] M.J. Krysmann, A. Kelarakis, P. Dallas, E.P. Giannelis, J. Am. Chem. Soc. 134 (2012) 747–750.
[26] H.T. Li, X.D. He, Z.H. Kang, H. Huang, Y. Liu, J.L. Liu, S.Y. Lian, C.H.A. Tsang, X.B. Yang, S.T. Lee, Angew. Chem. Int. Ed. 49 (2010) 4430–4434.
[27] C. Xie, B. Nie, L. Zeng, F.-X. Liang, M.-Z. Wang, L. Luo, M. Feng, Y. Yu, C.-Y. Wu, Y. Wu, S.-H. Yu, ACS Nano 8 (2014) 4015–4022.
[28] H.C. Zhang, H. Huang, H. Ming, H.T. Li, L.L. Zhang, Y. Liu, Z.H. Kang, J. Mater. Chem. 22 (2012) 10501–10506.
[29] H. Wang, Z. Wei, H. Matsui, S. Zhou, J. Mater. Chem. A 2 (2014) 15740–15745.
[30] X.-H. Li, J. Zhang, X. Chen, A. Fischer, A. Thomas, M. Antonietti, X. Wang, Chem. Mater. 23 (2011) 4344–4348.
[31] L. Zhao, F. Geng, F. Di, L.-H. Guo, B. Wan, Y. Yang, H. Zhang, G. Sun, RSC Adv. 4 (2014) 45768–45771.
[32] S.N. Baker, G.A. Baker, Angew. Chem. Int. Ed. 49 (2010) 6726–6744.
[33] T.Y. Ma, S. Dai, M. Jaroniec, S.Z. Qiao, Angew. Chem. Int. Ed. 53 (2014) 7281–7285.
[34] W.-J. Ong, L.-L. Tan, S.-P. Chai, S.-T. Yong, Chem. Commun. 51 (2015) 858–861.
[35] S. Yang, X. Feng, X. Wang, K. Müllen, Angew. Chem. Int. Ed. 50 (2011) 5339–5343.
[36] A. Tsuge, Y. Uwamino, T. Ishizuka, K. Suzuki, Appl. Spectrosc. 45 (1991) 1377–1380.
[37] L. Cao, X. Wang, J.M. Meziani, F. Lu, H. Wang, P.G. Luo, Y. Lin, B.A. Harruff, L.M. Veca, D. Murray, S.Y. Xie, Y.P. Sun, J. Am. Chem. Soc. 129 (2007) 11318–11319.
[38] H. Zhang, X. Fan, X. Quan, S. Chen, H. Yu, Environ. Sci. Technol. 45 (2011) 5731–5736.
[39] Y.J. Liu, X.Z. Jiang, Environ. Sci. Technol. 39 (2005) 8512–8517.
[40] R. Su, R. Tiruvalam, Q. He, N. Dimitratos, L. Kesavan, C. Hammond, J.A. Lopez-Sanchez, R. Bechstein, C.J. Kiely, G.J. Hutchings, F. Besenbacher, ACS Nano 6 (2012) 6284–6292.
[41] H. Wang, Y. Su, H. Zhao, H. Yu, S. Chen, Y. Zhang, X. Quan, Environ. Sci. Technol. 48 (2014) 11984–11990.
[42] H. Zhang, L.-H. Guo, L. Zhao, B. Wan, Y. Yang, J. Phys. Chem. Lett. 6 (2015) 958–963.
[43] L. Liu, T.D. Dao, R. Kodiyath, Q. Kang, H. Abe, T. Nagao, J. Ye, Adv. Funct. Mater. 24 (2014) 7754–7762.
[44] D. Jiang, W. Wang, S. Sun, L. Zhang, Y. Zheng, ACS Catal. 5 (2015) 613–621.
[45] G. Li, F. Wang, Q. Jiang, X. Gao, P. Shen, Angew. Chem. Int. Ed. 49 (2010) 3653–3656.